1

Potently neutralizing human antibodies that block SARS-CoV-2 receptor binding and protect

animals

AUTHORS: Seth J. Zost[1*], Pavlo Gilchuk[1*], James Brett Case[3], Elad Binshtein[1], Rita E. Chen[2,3],

Joseph X. Reidy[1], Andrew Trivette[1], Rachel S. Nargi[1], Rachel E. Sutton[1], Naveenchandra

Suryadevara[1], Lauren E. Williamson[4], Elaine C. Chen[4], Taylor Jones[1], Samuel Day[1], Luke

Myers[1], Ahmed O. Hassan[3], Natasha M. Kafai[2,3], Emma S. Winkler[2,3], Julie M. Fox[3], James J.

Steinhardt[6], Kuishu Ren[7], Yueh-Ming Loo[7], Nicole L. Kallewaard[7], David R. Martinez[5],

Alexandra Schäfer[5], Lisa E. Gralinski[5], Ralph S. Baric[5], Larissa B. Thackray[3], Michael S.

Diamond[2,3,8,9], Robert H. Carnahan[1,10**], James E. Crowe, Jr.[1,4,10**]

Affiliations:

[1]Vanderbilt Vaccine Center, Vanderbilt University Medical Center, Nashville, TN, 37232, USA

[2]Department of Pathology & Immunology, Washington University School of Medicine, St.

Louis, MO, 63110, USA

[3]Department of Medicine, Washington University School of Medicine, St. Louis, 63110, MO, USA

[4]Department of Pathology, Microbiology, and Immunology, Vanderbilt University Medical Center,

Nashville, TN, 37232, USA

[5]Department of Epidemiology, University of North Carolina at Chapel Hill, Chapel Hill, NC, 27599,

USA

[6]Antibody Discovery and Protein Engineering, BioPharmaceuticals R&D, AstraZeneca,

Gaithersburg, Maryland, 20878, USA

24   [7]Microbial Sciences, BioPharmaceuticals R&D, AstraZeneca, Gaithersburg, Maryland, 20878,

25   USA

26   [8]Department of Molecular Microbiology, Washington University School of Medicine, St. Louis,

27   MO, 63110, USA

28   [9]Andrew M. and Jane M. Bursky Center for Human Immunology and Immunotherapy Programs,

29   Washington University School of Medicine, St. Louis, MO, 63110, USA [10]Department of

30   Pediatrics, Vanderbilt University Medical Center, Nashville, TN, 37232, USA

31

32   **Contact information:**

33   **James E. Crowe, Jr., M.D.** *[LEAD CONTACT]*

34   Departments of Pediatrics, Pathology, Microbiology, and Immunology, and the Vanderbilt

35   Vaccine Center

36   **Mail:**

37   Vanderbilt Vaccine Center

38   11475 Medical Research Building IV

39   2213 Garland Avenue

40   Nashville, TN 37232-0417, USA

41   **Telephone**   (615) 343-8064

42   **Email**   james.crowe@vumc.org

43   **Additional Title Page Footnotes**

44   * These authors contributed equally

45   **Corresponding authors
46
47

48 **Keywords**: Coronavirus; SARS-CoV-2; SARS-CoV; COVID-19; Antibodies, Monoclonal;

49 Human; Adaptive Immunity.

50   **The COVID-19 pandemic is a major threat to global health for which there are only**

51   **limited medical countermeasures, and we lack a thorough understanding of mechanisms of**

52   **humoral immunity[1,2]. From a panel of monoclonal antibodies (mAbs) targeting the spike**

53   **(S) glycoprotein isolated from the B cells of infected subjects, we identified several mAbs**

54   **that exhibited potent neutralizing activity with IC_{50} values as low as 0.9 or 15 ng/mL in**

55   **pseudovirus or wild-type (*wt*) SARS-CoV-2 neutralization tests, respectively. The most**

56   **potent mAbs fully block the receptor-binding domain of S (S_{RBD}) from interacting with**

57   **human ACE2. Competition-binding, structural, and functional studies allowed clustering**

58   **of the mAbs into defined classes recognizing distinct epitopes within major antigenic sites**

59   **on the S_{RBD}. Electron microscopy studies revealed that these mAbs recognize distinct**

60   **conformational states of trimeric S protein. Potent neutralizing mAbs recognizing unique**

61   **sites, COV2-2196 and COV2-2130, bound simultaneously to S and synergistically**

62   **neutralized authentic SARS-CoV-2 virus. In two murine models of SARS-CoV-2 infection,**

63   **passive transfer of either COV2-2916 or COV2-2130 alone or a combination of both mAbs**

64   **protected mice from severe weight loss and reduced viral burden and inflammation in the**

65   **lung. These results identify protective epitopes on the S_{RBD} and provide a structure-based**

66   **framework for rational vaccine design and the selection of robust immunotherapeutic**

67   **cocktails.**

68

69   The S protein of SARS-CoV-2 is the molecular determinant of viral attachment, fusion, and

70   entry into host cells[3]. The cryo-EM structure of a prefusion-stabilized trimeric S protein

71   ectodomain ($S2P_{ecto}$) for SARS-CoV-2 reveals similar features to that of the SARS-CoV S

72   protein[4]. This type I integral membrane protein and class I fusion protein possesses an N-

73   terminal subunit (S1) that mediates binding to receptor and a C-terminal subunit (S2) that

74   mediates virus–cell membrane fusion. The S1 subunit contains an N-terminal domain (S_{NTD}) and

75   a receptor-binding domain (S_{RBD}). SARS-CoV-2 and SARS-CoV, which share approximately

76   78% sequence identity in their genomes[1] both use human angiotensin-converting enzyme 2

77   (hACE2) as an entry receptor[5-7]. Previous studies of human immunity to other high-

78   pathogenicity zoonotic betacoronaviruses including SARS-CoV[8-12] and Middle East respiratory

79   syndrome (MERS)[13-22] showed that Abs to the viral surface spike (S) glycoprotein mediate

80   protective immunity. The most potent S protein-specific mAbs appear to neutralize

81   betacoronaviruses by blocking attachment of virus to host cells by binding to the region on S_{RBD}

82   that directly mediates engagement of the receptor. It is likely that human Abs have promise for

83   use in modifying disease during SARS-CoV-2 infection, when used for prophylaxis, post-

84   exposure prophylaxis, or treatment of SARS-CoV-2 infection[23]. Many studies including

85   randomized controlled trials evaluating convalescent plasma and one trial evaluating

86   hyperimmune immunoglobulin are ongoing, but it is not yet clear whether such treatments can

87   reduce morbidity or mortality[24].

88

89   We isolated a large panel of SARS-CoV-2 S protein-reactive mAbs from the B cells of two

90   individuals who were previously infected with SARS-CoV-2 in Wuhan China[25]. A subset of

91   those antibodies bound to the receptor-binding domain of S (S_{RBD}) and exhibited neutralizing

92   activity in a rapid screening assay with authentic SARS-CoV-2[25]. Here, we defined the antigenic

93   landscape of SARS-CoV-2 and determined which sites of S_{RBD} are the target of protective mAbs.

94   We tested a panel of 40 anti-S human mAbs we previously pre-selected by a rapid neutralization

95   screening assay in a quantitative focus reduction neutralization test (FRNT) with SARS-CoV-2

96   strain WA1/2020. These assays revealed the panel exhibited a range of half-maximal inhibitory

97   concentration (IC_{50}) values, from 15 to over 4,000 ng/mL (visualized as a heatmap in Fig. 1a,

98   values shown in Extended Data Table 1, and full curves shown in Extended Data Fig. 1). We

99   hypothesized that many of these S_{RBD}-reactive mAbs neutralize virus infection by blocking S_{RBD}

100   binding to hACE2. Indeed, most neutralizing mAbs we tested inhibited the interaction of hACE2

101   with trimeric S protein directly (Fig. 1a, Extended Data Fig. 2). Consistent with these results,

102   these mAbs also bound strongly to a trimeric S ectodomain ($S2P_{ecto}$) protein or monomeric S_{RBD}

103   (Fig. 1a, Extended Data Fig. 3). We evaluated whether $S2P_{ecto}$ or S_{RBD} binding or hACE2-

104   blocking potency predicted binding neutralization potency independently, but none of these

105   measurements correlated with neutralization potency (Fig. 1b-d). However, each of the mAbs in

106   the highest neutralizing potency tier (IC_{50}<150 ng/mL) also revealed strongest blocking activity

107   against hACE2 (IC_{50}< 150 ng/mL) and exceptional binding activity (EC_{50}< 2 ng/mL) to $S2P_{ecto}$

108   trimer and S_{RBD} (Fig. 1e). Representative neutralization curves for two potently neutralizing

109   mAbs designated COV2-2196 and COV2-2130 are shown in (Fig. 1f). Potent neutralization was

110   confirmed using pseudovirus neutralization assays, which revealed far more sensitive

111   neutralization phenotypes than *wt* virus and demonstrated a requirement for the use of live virus

112   assays for assessment of mAb potency (Fig. 1g). Both of these mAbs bound strongly to $S2P_{ecto}$

113   trimer and fully blocked hACE2 binding (Fig. 1h-i).

114

115   We next defined the major antigenic sites on S_{RBD} for neutralizing mAbs by competition-binding

116   analysis. We first used a biolayer interferometry-based competition assay with a minimal S_{RBD}

117   domain to screen for mAbs that competed for binding with the potently neutralizing mAb COV2-

118   2196 or a recombinant version of the previously described SARS-CoV mAb CR3022, which

119   recognizes a conserved cryptic epitope[10,26]. We identified three major groups of competing mAbs

120   (Fig. 2a). The largest group of mAbs blocked COV2-2196 but not rCR3022, while some mAbs

121   were blocked by rCR3022 but not COV2-2196. Two mAbs, including COV2-2130, were not

122   blocked by either reference mAb. Most mAbs competed with hACE2 for binding, suggesting

123   that they bound near the hACE2 binding site of the S_{RBD}. We used COV2-2196, COV2-2130,

124   and rCR3022 in an ELISA-based competition-binding assay with trimeric S2P$_{ecto}$ protein and

125   also found that S_{RBD} contained three major antigenic sites, with some mAbs likely making

126   contacts in more than one site (Fig. 2b). Most of the potently neutralizing mAbs directly

127   competed for binding with COV2-2196.

128

129   Since COV2-2196 and COV2-2130 did not compete for binding to S_{RBD}, we assessed if these

130   mAbs synergize for virus neutralization, a phenomenon previously observed for SARS-CoV

131   mAbs[10]. We tested combination responses (see dose-response neutralization matrix, Fig. 2c) in

132   the FRNT using SARS-CoV-2 and compared these experimental values with the expected

133   responses calculated by synergy scoring models[27]. The comparison revealed that the combination

134   of COV2-2196 + COV2-2130 was synergistic (with a synergy score of 17.4, where any score of

135   >10 indicates synergy). The data in Fig. 2c shows the dose-response synergy matrix and

136   demonstrates that a combined mAb dose of 79 ng/mL in the cocktail (16 ng/mL of COV2-2196

137   and 63 ng/mL of COV2-2130) had the same activity as 250 ng/mL of each individual mAb (see

138   Fig. 2c). This finding shows that using a cocktail the dose of each mAb can be reduced by more

139   than three-fold to achieve the same potency of virus neutralization *in vitro*.

140

141   We next defined the epitopes recognized by representative mAbs in the two major competition-

142   binding groups that synergize for neutralization. We performed mutagenesis studies of the S_{RBD}

143   using alanine or arginine substitution to determine critical residues for binding of neutralizing

144   mAbs (Extended Data Fig. 4). Loss of binding studies revealed F486A or N487A as critical

145   residues for COV2-2196 and N487A as a critical residue for COV2-2165, which compete with

146   one another for binding, and likewise mutagenesis studies for COV2-2130 using K444A and

147   G447R mutants defined these residues as critical for recognition (Fig. 3a). Previous structural

148   studies have defined the interaction between the S_{RBD} and hACE2 (Fig. 3b)[28]. Most of the

149   interacting residues in the S_{RBD} are contained within a 60-amino-acid linear peptide that defines

150   the hACE2 recognition motif (Fig. 3c). We next tested binding of human mAbs to this minimal

151   peptide and found that potent neutralizing members of the largest competition-binding group

152   including COV2-2196, COV2-2165, and COV2-2832 recognized this peptide (Fig. 3c),

153   suggesting these mAbs make critical contacts within the hACE2 recognition motif.

154

155   We used negative-stain electron microscopy of S2P$_{ecto}$ trimer/Fab complexes to structurally

156   determine the epitopes for these mAbs. The potently neutralizing antibodies COV2-2196 and

157   COV2-2165 bound to the hACE2 recognition motif of S_{RBD} and recognized the 'open'

158   conformational state of the S2P$_{ecto}$ trimer (Fig. 3d). The mode of engagement of these two

159   antibodies differed, however, as the binding pose and the angle relative to the spike 'body' for

160   one was different compared to the other. COV2-2130, which represents the second competition-

161   binding group, bound to the RBD in the S2P$_{ecto}$ trimer in the 'closed' position (Fig. 3d). Since

162   COV2-2196 and COV2-2130 did not compete for binding, we attempted to make complexes of

163   both Fabs bound at the same time to the S2P$_{ecto}$ trimer. We found that both Fabs bound

164   simultaneously when the S2P$_{ecto}$ trimer was in the open position, indicating that COV2-2130 can

165   recognize the S$_{RBD}$ in both conformations (Fig. 3e). Overlaying the two-Fab complex with the

166   structure of the RBD:CR3022 complex[26], we observed that these antibodies bind to three distinct

167   sites on S$_{RBD}$, as predicted based on our competition-binding studies (Fig. 3f).

168

169   Next, we tested the prophylactic efficacy of COV2-2196 or COV2-2130 monotherapy or a

170   combination of COV2-2196 + COV2-2130 in a newly developed SARS-CoV-2 infection model

171   in BALB/c mice in which hACE2 is expressed in the lung after intranasal adenovirus (AdV-

172   hACE2) transduction. In this relatively stringent disease model, we also administered a single

173   dose of anti-Ifnar1 antibody to augment virus infection and pathogenesis, which results in a

174   disseminated interstitial pneumonia (A. Hassan and M. Diamond, submitted for publication). We

175   passively transferred a single dose of mAb COV2-2196 (10 mg/kg), COV2-2130 (10 mg/kg), a

176   combination of COV2-2196 + COV2-2130 (5 mg/kg each), or an isotype control mAb (10

177   mg/kg) to AdV-hACE2-transduced mice one day before intranasal challenge with 4 x 10^5 PFU of

178   SARS-CoV-2. Prophylaxis with COV2-2196 or COV2-2130 or their combination prevented

179   severe SARS-CoV-2-induced weight loss through the first week of infection (Fig. 4a).

180   Viral RNA levels were reduced significantly at 7 dpi in the lung and distant sites including the

181   heart and spleen (Fig. 4b). The expression of interferon gamma (INF-g), IL-6, CXCL10 and

182   CCL2 cytokine and chemokine genes, which are indicators of inflammation, also was reduced in

183   the lung of treated mice at 7 dpi —the peak of the disease (Fig. 4c).

184

185   We also tested COV2-2196 or COV2-2130 or their combination for prophylactic efficacy in an

186   immunocompetent model using a mouse-adapted (MA) SARS-CoV-2 virus[29] (Fig. 4d). *In vitro*

187   tests showed that the IC_{50} values for neutralization were comparable for the *wt* and MA SARS-

188   CoV-2 viruses for these mAbs (data not shown). Each of the mAb treatments delivered at a dose

189   of 200 µg/mouse (~ 8 mg/kg) reduced viral RNA levels up to 10^5-fold at 2 dpi in the lung when

190   compared to the isotype control group (Fig. 4e, left). Concordantly, all animals from COV2-2196

191   and COV2-2196 + COV2-2130 treatment group and 8 of 10 animals from COV2-2130 treatment

192   no longer had infectious virus at 2 dpi in the lung as measured by plaque titer of lung tissue (Fig.

193   4e, right). Collectively, these results in mice suggested that COV2-2196 or COV2-2130 alone or

194   in combination are promising candidates for treatment or prevention of COVID-19.

195

196   Here, we defined the antigenic landscape for a large panel of highly potent mAbs against SARS-

197   CoV-2. These detailed studies and the screening studies that identified this panel of mAbs from a

198   larger panel of hundreds[25] demonstrate that although diverse human neutralizing antibodies are

199   elicited by natural infection with SARS-CoV-2, only a small subset of those mAbs are of high

200   potency (IC_{50}<50 ng/mL against live SARS-CoV-2 virus), and therefore, suitable for therapeutic

201   development. Biochemical and structural analysis of these potent mAbs defined three principal

202   antigenic sites of vulnerability to neutralization by human mAbs elicited by natural infection

203   with SARS-CoV on the S_{RBD}. Representative mAbs from the two most potent antigenic sites

204   were shown to synergize *in vitro* and protect as an *in vivo* cocktail. This finding reveals critical

205   features of effective humoral immunity to SARS-CoV-2 and suggests that the role of synergistic

206   neutralization activity in polyclonal responses should be explored further. Moreover, as SARS-

207   CoV-2 continues to circulate, population immunity elicited by natural infection may start to

208   select for antigenic variants that escape from the selective pressure of neutralizing antibodies,

209   reinforcing the need to target multiple epitopes of S protein in vaccines or immunotherapeutics.

210   The common S gene variants across the globe reported to date are located at positions D614G,

211   V483A, L5F, Q675H, H655Y and S939F[30], far away from the amino acid variants at residues

212   486 or 487 identified in our mutation studies for the lead mAbs studied here. Rationally-selected

213   therapeutic cocktails like the one described here might offer even greater resistance to SARS-

214   CoV-2 escape. These studies set the stage for preclinical evaluation and development of the

215   identified mAbs as candidates for use as COVID-19 immunotherapeutics in humans.

216

217   **Data availability.** The EM maps have been deposited at the Electron Microscopy Data Bank

218   with accession codes EMBD 21965 (S2P$_{ecto}$ apo), EMD-21974 (S2P$_{ecto}$ + Fab COVs-2165),

219   EMD-21975 (S2P$_{ecto}$ + Fab COVs-2196), EMD-21976 (S2P$_{ecto}$ + Fab COVs-2130) and EMD-

220   21977 (S2P$_{ecto}$ + Fab COV2-2196 + Fab COV2-2130). Materials reported in this study will be

221   made available but may require execution of a Materials Transfer Agreement.

222

239   content is solely the responsibility of the authors and does not necessarily represent the official views of

240   the U.S. government or the other sponsors.

241

242   **Author contributions.** Conceived of the project: S.J.Z., P.G., R.H.C., L.B.T., M.S.D., J.E.C.;

243   Obtained funding: J.E.C. and M.S.D. Performed laboratory experiments: S.J.Z., P.G., J.B.C.,

244   E.B., R.E.C., J.X.R., A.T., R.S.N., R.E.S., N.S., L.E.W., A.O.H., N.M.K., E.W., J.M.F., L.B.T.,

245   J.J.S., K.R., Y.-M.L., A.S., L.E.G., D.R.M.; Performed computational work: E.C.C., T.J., S.D.,

246   L.M.; Supervised research: N.L.K, M.S.D., L.B.T., R.S.B., R.H.C., J.E.C. Wrote the first draft of

247   the paper: S.J.Z., P.G., R.H.C., J.E.C.; All authors reviewed and approved the final manuscript.

248

249   **Competing interests.** R.S.B. has served as a consultant for Takeda and Sanofi Pasteur on issues related

250   to vaccines. M.S.D. is a consultant for Inbios, Vir Biotechnology, NGM Biopharmaceuticals, Eli Lilly,

251   and is on the Scientific Advisory Board of Moderna, a past recipient of unrelated research grant from

252   Moderna and a current recipient of an unrelated research grant Emergent BioSolutions.

253   J.E.C. has served as a consultant for Sanofi and is on the Scientific Advisory Boards of CompuVax and

254   Meissa Vaccines, is a recipient of previous unrelated research grants from Moderna and Sanofi and is

255   Founder of IDBiologics, Inc. Vanderbilt University has applied for patents concerning SARS-CoV-2

256   antibodies that are related to this work. AstraZeneca has filed patents for materials/findings related to

257   this work. J.J.S., K.R., Y.-M.L., and N.L.K. are employees of AstraZeneca and currently hold

258   AstraZeneca stock or stock options. All other authors declared no competing interests.

259

260   **Additional information**
261
262   **Supplementary information** is available for this paper.
263

264   **Correspondence and requests for materials** should be addressed to J.E.C.

REFERENCES

1. Zhou, P.*, et al.* A pneumonia outbreak associated with a new coronavirus of probable bat origin. *Nature* **579**, 270-273 (2020).

2. Zhu, N.*, et al.* A novel coronavirus from patients with pneumonia in China, 2019. *N Engl J Med* **382**, 727-733 (2020).

3. Pillay, T.S. Gene of the month: the 2019-nCoV/SARS-CoV-2 novel coronavirus spike protein. *J Clin Pathol* (2020).

4. Wrapp, D.*, et al.* Cryo-EM structure of the 2019-nCoV spike in the prefusion conformation. *Science* **367**, 1260-1263 (2020).

5. Wan, Y., Shang, J., Graham, R., Baric, R.S. & Li, F. Receptor recognition by the novel Coronavirus from Wuhan: an Analysis Based on Decade-Long Structural Studies of SARS Coronavirus. *J Virol* **94**(2020).

6. Hoffmann, M.*, et al.* SARS-CoV-2 cell entry depends on ACE2 and TMPRSS2 and is blocked by a clinically proven protease inhibitor. *Cell* **181**, 271-280 e278 (2020).

7. Li, W.*, et al.* Angiotensin-converting enzyme 2 is a functional receptor for the SARS coronavirus. *Nature* **426**, 450-454 (2003).

288

289 8. Sui, J., *et al.* Potent neutralization of severe acute respiratory syndrome (SARS)

290 coronavirus by a human mAb to S1 protein that blocks receptor association. *Proc Natl*

291 *Acad Sci U S A* **101**, 2536-2541 (2004).

292

293 9. ter Meulen, J., *et al.* Human monoclonal antibody as prophylaxis for SARS coronavirus

294 infection in ferrets. *Lancet* **363**, 2139-2141 (2004).

295

296 10. ter Meulen, J., *et al.* Human monoclonal antibody combination against SARS coronavirus:

297 synergy and coverage of escape mutants. *PLoS Med* **3**, e237 (2006).

298

299 11. Zhu, Z., *et al.* Potent cross-reactive neutralization of SARS coronavirus isolates by human

300 monoclonal antibodies. *Proc Natl Acad Sci U S A* **104**, 12123-12128 (2007).

301

302 12. Rockx, B., *et al.* Structural basis for potent cross-neutralizing human monoclonal antibody

303 protection against lethal human and zoonotic severe acute respiratory syndrome

304 coronavirus challenge. *J Virol* **82**, 3220-3235 (2008).

305

306 13. Chen, Z., *et al.* Human neutralizing monoclonal antibody inhibition of Middle East

307 respiratory syndrome coronavirus replication in the common marmoset. *J Infect Dis* **215**,

308 1807-1815 (2017).

309

310   14.   Choi, J.H., *et al.* Characterization of a human monoclonal antibody generated from a B-cell specific for a prefusion-stabilized spike protein of Middle East respiratory syndrome coronavirus. *PLoS One* **15**, e0232757 (2020).

314   15.   Niu, P., *et al.* Ultrapotent human neutralizing antibody repertoires against Middle East respiratory syndrome coronavirus from a recovered patient. *J Infect Dis* **218**, 1249-1260 (2018).

318   16.   Wang, L., *et al.* Importance of neutralizing monoclonal antibodies targeting multiple antigenic sites on the Middle East respiratory syndrome coronavirus spike glycoprotein to avoid neutralization escape. *J Virol* **92**(2018).

322   17.   Wang, N., *et al.* Structural definition of a neutralization-sensitive epitope on the MERS-CoV S1-NTD. *Cell Rep* **28**, 3395-3405 e3396 (2019).

325   18.   Zhang, S., *et al.* Structural definition of a unique neutralization epitope on the receptor-binding domain of MERS-CoV spike glycoprotein. *Cell Rep* **24**, 441-452 (2018).

328   19.   Corti, D., *et al.* Prophylactic and postexposure efficacy of a potent human monoclonal antibody against MERS coronavirus. *Proc Natl Acad Sci U S A* **112**, 10473-10478 (2015).

331   20.   Jiang, L., *et al.* Potent neutralization of MERS-CoV by human neutralizing monoclonal antibodies to the viral spike glycoprotein. *Sci Transl Med* **6**, 234ra259 (2014).

333

334   21.   Tang, X.C.*, et al.* Identification of human neutralizing antibodies against MERS-CoV and

335   their role in virus adaptive evolution. *Proc Natl Acad Sci U S A* **111**, E2018-2026 (2014).

336

337   22.   Ying, T.*, et al.* Exceptionally potent neutralization of Middle East respiratory syndrome

338   coronavirus by human monoclonal antibodies. *J Virol* **88**, 7796-7805 (2014).

339

340   23.   Jiang, S., Hillyer, C. & Du, L. Neutralizing antibodies against SARS-CoV-2 and other

341   human coronaviruses. *Trends Immunol* **41**, 355-359 (2020).

342

343   24.   Valk, S.J.*, et al.* Convalescent plasma or hyperimmune immunoglobulin for people with

344   COVID-19: a rapid review. *Cochrane Database Syst Rev* **5**, CD013600 (2020).

345

346   25.   Zost, S.J.*, et al.* Rapid isolation and profiling of a diverse panel of human monoclonal

347   antibodies targeting the SARS-CoV-2 spike protein. *bioRxiv*, 2020.2005.2012.091462

348   (2020).

349

350   26.   Yuan, M.*, et al.* A highly conserved cryptic epitope in the receptor binding domains of

351   SARS-CoV-2 and SARS-CoV. *Science* **368**, 630-633 (2020).

352

353   27.   Ianevski, A., He, L., Aittokallio, T. & Tang, J. SynergyFinder: a web application for

354   analyzing drug combination dose-response matrix data. *Bioinformatics* **33**, 2413-2415

355   (2017).

356

357 28. Lan, J.*, et al.* Structure of the SARS-CoV-2 spike receptor-binding domain bound to the

358   ACE2 receptor. *Nature* **581**, 215-220 (2020).

359

360 29. Dinnon, K.H.*, et al.* A mouse-adapted SARS-CoV-2 model for the evaluation of COVID-

361   19 medical countermeasures. *bioRxiv*, 2020.2005.2006.081497 (2020).

362

363 30. Laha, S.*, et al.* Characterizations of SARS-CoV-2 mutational profile, spike protein stability

364   and viral transmission. *bioRxiv*, 2020.2005.2003.066266 (2020).

365

366

367 **Figure Legends:**

368 **Figure 1. Functional characteristics of neutralizing SARS-CoV-2 mAbs.**

369 **a.** Heatmap of mAb neutralization activity, hACE2 blocking activity, and binding to either

370 trimeric S2Pecto protein or monomeric SRBD. MAbs are ordered by neutralization potency

371 (highest at the top, lowest at the bottom). Dashed lines indicate the 13 antibodies with a

372 neutralization IC50 value lower than 150 ng/mL for wt virus. IC50 values are visualized for viral

373 neutralization and hACE2 blocking, while EC50 values are visualized for binding. A

374 recombinant form of the cross-reactive SARS-CoV SRBD mAb CR3022 is shown as a positive

375 control, while the anti-dengue mAb 2D22 is shown as a negative control. Data are representative

376 of at least 2 independent experiments, each performed in technical duplicate. No inhibition

377 indicates an IC50 value of >10,000 ng/mL, while no binding indicates an EC50 value of >10,000

378 ng/mL.

379   **b-d.** Correlation of hACE2 blocking, S2Pecto trimer binding, or SRBD binding of mAbs with

380   their neutralization activity. R2 values are shown for linear regression analysis of log-

381   transformed values. Purple circles indicate mAbs with a neutralization IC50 value lower than

382   150 ng/mL.

383   **e.** Correlation of hACE2 blocking and S2Pecto trimer binding. R2 values are shown for linear

384   regression analysis of log-transformed values.

385   **f.** Neutralization curves for COV2-2196 and COV2-2130 in a neutralization assay against

386   authentic SARS-CoV-2 virus. Calculated IC50 values are denoted on the graph. Error bars

387   denote the standard deviation of each point. Data are representative of at least 2 independent

388   experiments, each performed in technical duplicate.

389   **g.** Neutralization curves for COV2-2196 and COV2-2130 in a pseudovirus neutralization assay.

390   Error bars denote the standard deviation of each point. Values shown are technical duplicates

391   from a single experiment. Calculated IC50 values from a minimum of 6 experiments are denoted

392   on the graph.

393   **h.** hACE2 blocking curves for COV2-2196, COV2-2130, and the non-blocking SARS-CoV mAb

394   rCR3022 in the hACE2 blocking ELISA. Calculated IC50 values are denoted on the graph. Error

395   bars denote the standard deviation of each point. Values shown are technical triplicates from a

396   representative experiment repeated twice.

397   **i.** ELISA binding of COV2-2196, COV2-2130, and rCR3022 to trimeric S2Pecto. Calculated

398   EC50 values are denoted on the graph. Error bars denote the standard deviation of each point.

399   Values shown are technical triplicates from a representative experiment repeated twice.

400

401

402

403 **Figure 2. Epitope mapping of mAbs by competition-binding analysis and synergistic**

404 **neutralization by a pair of mAbs.**

405 **a.** Left: biolayer interferometry-based competition binding assay measuring the ability of mAbs

406 to prevent binding of reference mAbs COV2-2196 and rCR3022 to RBD fused to mouse Fc

407 (RBD-mFc) loaded onto anti-mouse Fc biosensors. Values in squares are % of binding of the

408 reference mAb in the presence of the competing mAb relative to a mock-competition control.

409 Black squares denote full competition (<33% of binding relative to no-competition control),

410 while white squares denote no competition (>67% of binding relative to no-competition control).

411 Right: biolayer interferometry-based competition binding assay measuring the ability of mAbs to

412 prevent binding of hACE2. Values denote % binding of hACE2, normalized to hACE2 binding

413 in the absence of competition. Red color denotes competition of mAb with hACE2.

414 **b.** Competition of neutralizing mAb panel with reference mAbs COV2-2130, COV2-2196, or

415 rCR3022. Reference mAbs were biotinylated and binding of reference mAbs to trimeric S2Pecto

416 was measured in the presence of saturating amounts of each mAb in a competition ELISA.

417 ELISA signal for each reference mAb was normalized to the signal in the presence of the non-

418 binding anti-dengue mAb 2D22. Black denotes full competition (<25% binding of reference

419 mAb), grey denotes partial competition (25-60% binding of reference mAb), and white denotes

420 no competition (>60% binding of reference mAb).

421 **c.** Neutralization dose-response matrix of wild-type SARS-CoV-2 by COV2-2196 and COV2-

422 2130. Axes denote the concentration of each mAb. Experiment was performed in technical

423 triplicate. Shown is a representative experiment that was performed in technical triplicate. %

424 neutralization for each combination of mAbs is shown in each square. A white-to-red heatmap

425   denotes 0% neutralization to 100% neutralization, respectively. **d.** Synergy map calculated based

426   on the SARS-CoV-2 neutralization in the above panel. Red color denotes areas where synergistic

427   neutralization was observed, and a black box denotes the area of maximal synergy between the

428   two mAbs.

429

430   **Figure 3. Epitope identification and structural characterization of mAbs.**

431   **a.** Identification of critical contact residues by alanine and arginine mutagenesis. Top: binding of

432   COV2-2130 (gold), COV2-2165 (maroon) or COV2-2196 (dark purple) to wild-type (wt) or

433   mutant SRBD constructs measured by biolayer interferometry. Shown on y-axis is the response

434   normalized to the signal observed for binding to wt SRBD. Bottom: representative binding

435   curves for COV2-2196 to wt or SRBD constructs with critical contact residues mutated.

436   **b.** Crystal structure of SARS-CoV-2 (blue) and hACE2 (green) (PDB (6M0J). The hACE2

437   recognition motif is colored orange. Critical contact residues for COV2-2130 are shown as gold

438   spheres, while critical contact residues for COV2-2196 are shown as purple spheres.

439   **c.** ELISA binding of mAbs to the 60-amino-acid hACE2 recognition motif. r2D22, an anti-

440   dengue mAb, is shown as a negative control. Bottom: structure of hACE2 recognition motif in

441   orange with COV2-2196 critical contact residues shown in purple.

442   **d.** Single-Fab:S2Pecto trimer complexes visualized by negative-stain electron microscopy for

443   COV2-2130 (gold), COV2-2165 (maroon), or COV2-2196 (dark purple). The RBD is shown in

444   blue and the S N-terminal domain (NTD) is shown in red. Electron density is shown in grey.

445   Trimer state (open or closed) is denoted for each complex. Representative 2D class averages for

446   each complex are shown at the bottom (box size 128 pixel).

447   **e.** COV2-2130 and COV2-2196 Fabs in complex with S2Pecto trimer. Simultaneous binding of

448   COV2-2130 (gold) and COV2-2196 (purple) Fabs to S2Pecto trimer. Electron density is shown

449   in grey. Trimer state (open or closed) is denoted. Representative 2D class averages for the

450   complexes are shown at the bottom (box size 128 pixels). All images were made with Chimera.

451   f. Competition-binding analysis visualized on S2Pecto trimer. The CR3022 crystal structure was

452   docked into the double-Fab:S2Pecto trimer structure. CR3022 is shown in cyan. Bottom: a

453   quantitative Venn diagram notes the number of mAbs in each competition group and the overlap

454   between groups.

455

456   **Figure 4. Protective efficacy of neutralizing human mAbs against SARS-CoV-2 infection.**

457   **a.** SARS-CoV-2 challenge model. Ten to eleven-week-old BALB/c mice (two experiments of 4-

458   5 mice per group) were treated with anti-Ifnar1 mAb and transduced with AdV-hACE2 via the

459   i.n. route one day later. After four days, mice were treated via the i.p. route with 200 μg of mAbs

460   CoV2-2196, -2130, or combination (1:1 ratio) or isotype control mAb. One day later, SARS-

461   CoV-2 was inoculated via the i.n. route. Tissues were harvested at 7 dpi for analysis (c, d).

462   **b.** Body weight change of mice in panel a. (two-way ordinary ANOVA with Tukey's post-test:

463   **** $P < 0.0001$).

464   **c.** Viral burden in the lung, spleen and heart was measured by RT-qPCR: Kruskal-Wallis

465   ANOVA with Dunn's post-test (*, $P < 0.05$, ** $P < 0.01$, *** $P < 0.001$, **** $P < 0.0001$). The

466   dashed line indicates the assay limit of detection.

467   **d.** Cytokine and chemokine gene expression was measured by qPCR analysis. Kruskal-Wallis

468   ANOVA with Dunn's post-test (*, $P < 0.05$, ** $P < 0.01$, *** $P < 0.001$).

469   **e.** MA-SARS-CoV-2 challenge model. Twelve-week-old BALB/c mice (n=10) were inoculated

470   with 105 PFU of MA-SARS-CoV-2 via the i.n. route. Body weight change of mice is shown.

471   **f.** Viral burden in the lung was measured at 2 dpi by RT-qPCR (left) or plaque assay (right) from

472   (e): Kruskal-Wallis ANOVA with Dunn's post-test (*** P < 0.001, **** P < 0.0001).

473

474   **Supplementary Information**

475
476   **Extended Data Figure. 1. SARS-CoV-2 neutralization curves for mAb panel.** Neutralization

477   of authentic SARS-CoV-2 by human mAbs. Mean ± SD of technical duplicates is shown. Data

478   represent one of two or more independent experiments

479

480   **Extended Data Figure 2. Inhibition curves for mAb inhibition of S2P$_{ecto}$ binding to hACE2.**

481   Blocking of hACE2 binding to S2P$_{ecto}$ by anti-SARS-CoV-2 neutralizing human mAbs. Mean ±

482   SD of triplicates of one experiment is shown. Antibodies CR3022 and 2D22 served as controls.

483

484   **Extended Data Figure. 3. ELISA binding of anti-SARS-CoV-2 neutralizing human mAbs to**

485   **trimeric S$_{RBD}$, S2P$_{ecto}$, or SARS-CoV S2P$_{ecto}$ antigen.** Mean ± SD of triplicates and

486   representative of two experiments are shown. Antibodies CR3022 and 2D22 served as controls.

487

488   **Extended Data Figure. 4. Mapping of mAb critical contact residues by alanine and arginine**

489   **mutagenesis and biolayer interferometry.**

490   **a.** *Left*: Response values for mAb binding to *wt* or mutant S$_{RBD}$ constructs normalized to *wt*.

491   Asterisks denote residues where increased dissociation of mAb was observed, likely indicating

492   the residue is proximal to mAb epitope. *Right*: full response curves for mAb association and

493   dissociation with *wt* or mutant S_{RBD} constructs.

494   **b.** Structure of the RBD highlighting the critical contact residues for several mAbs and their

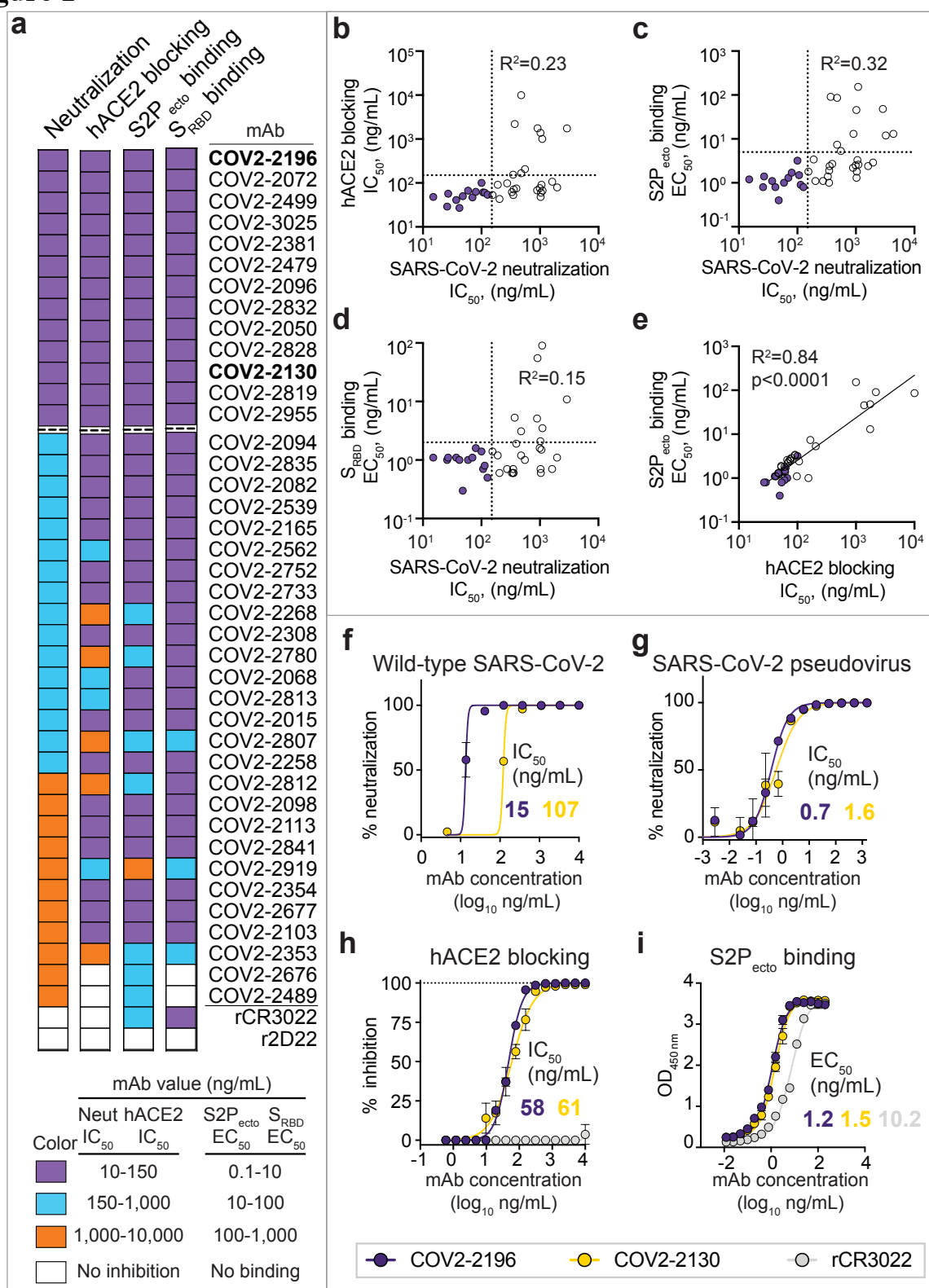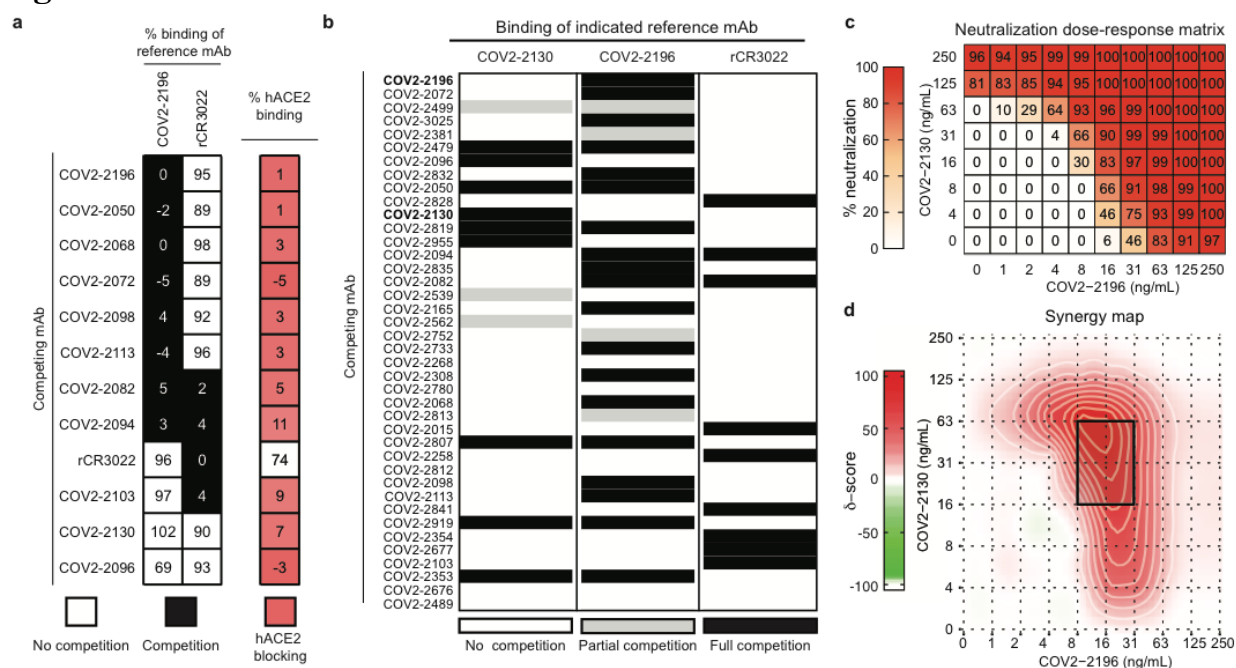495   location on the structure.
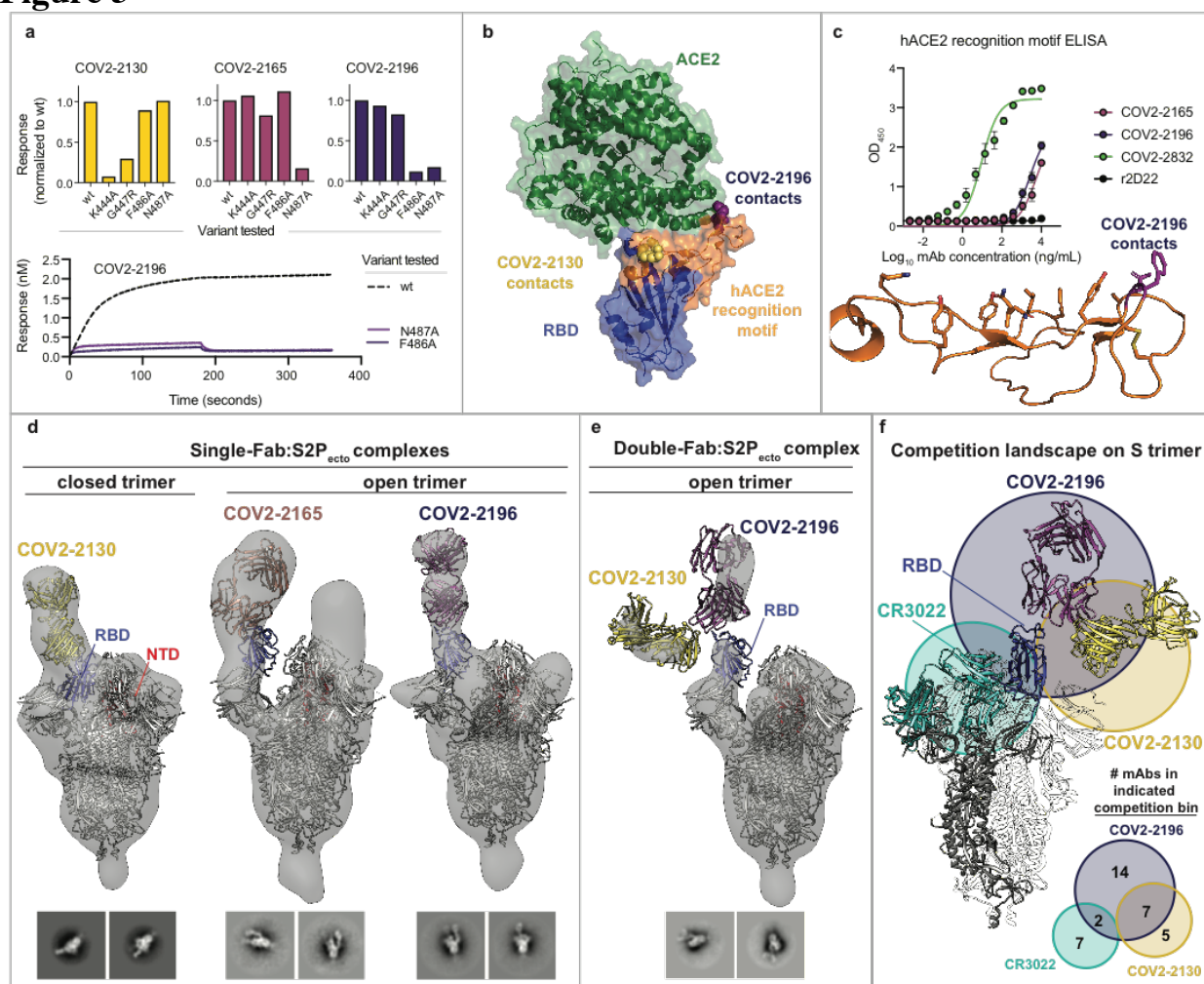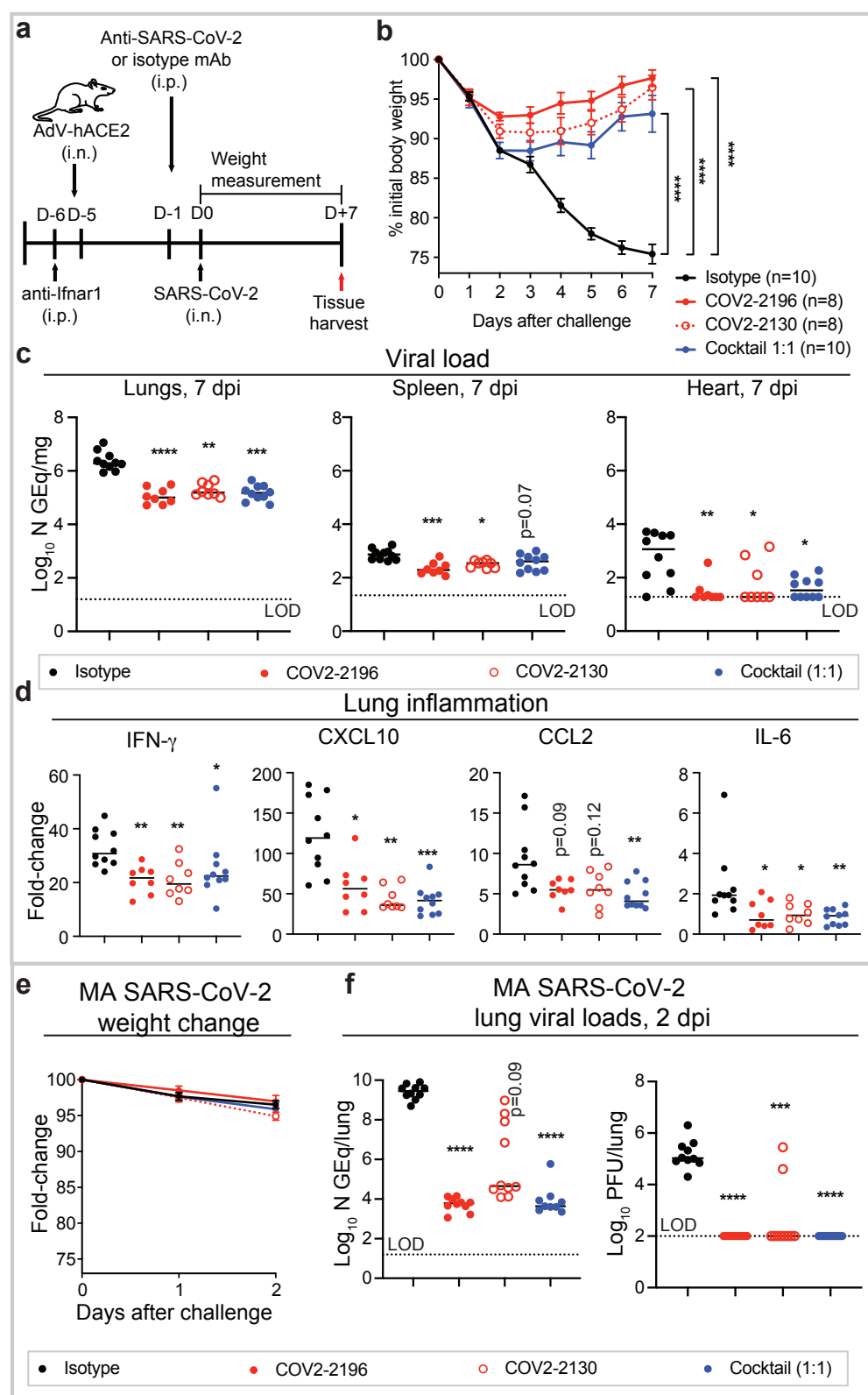
496

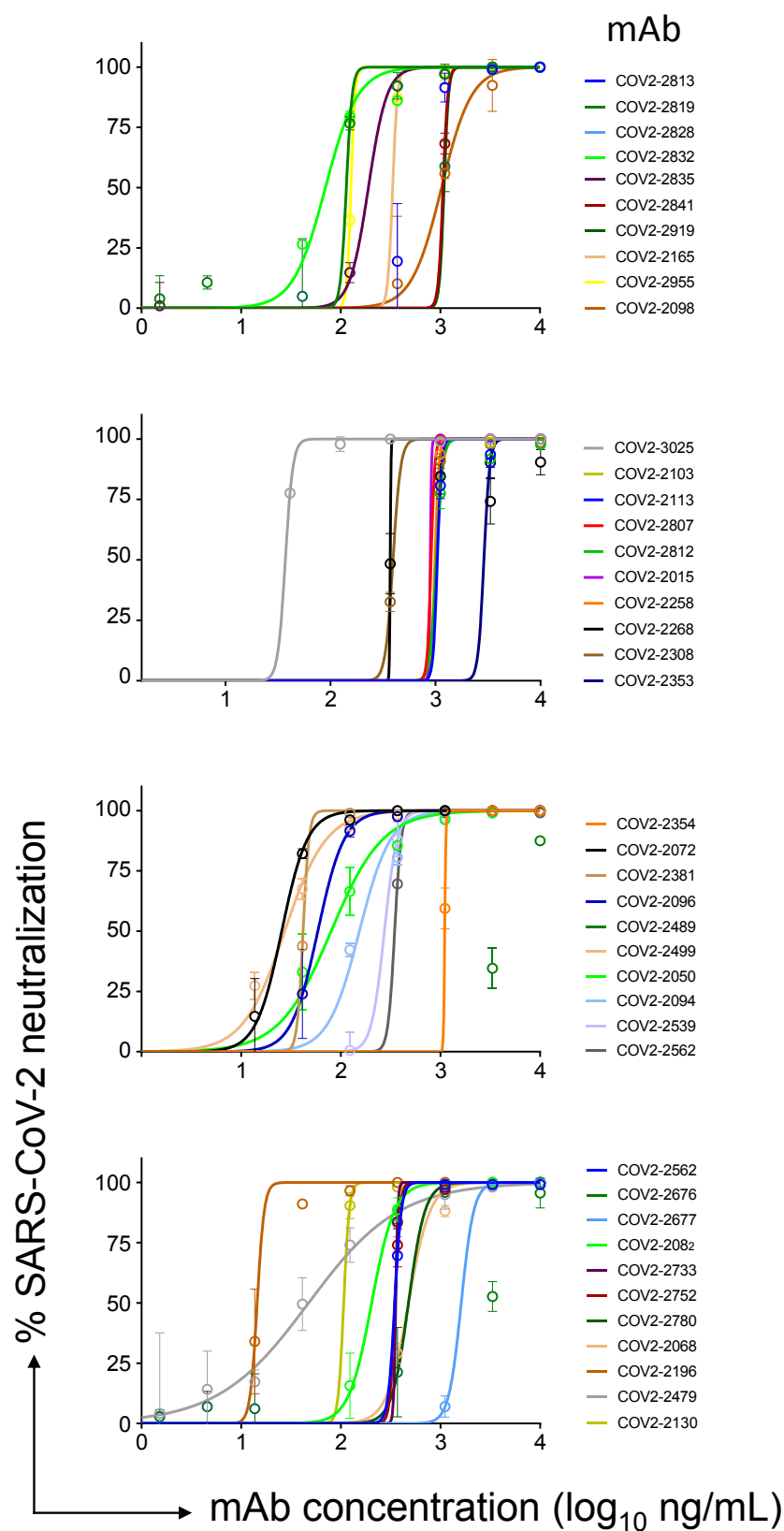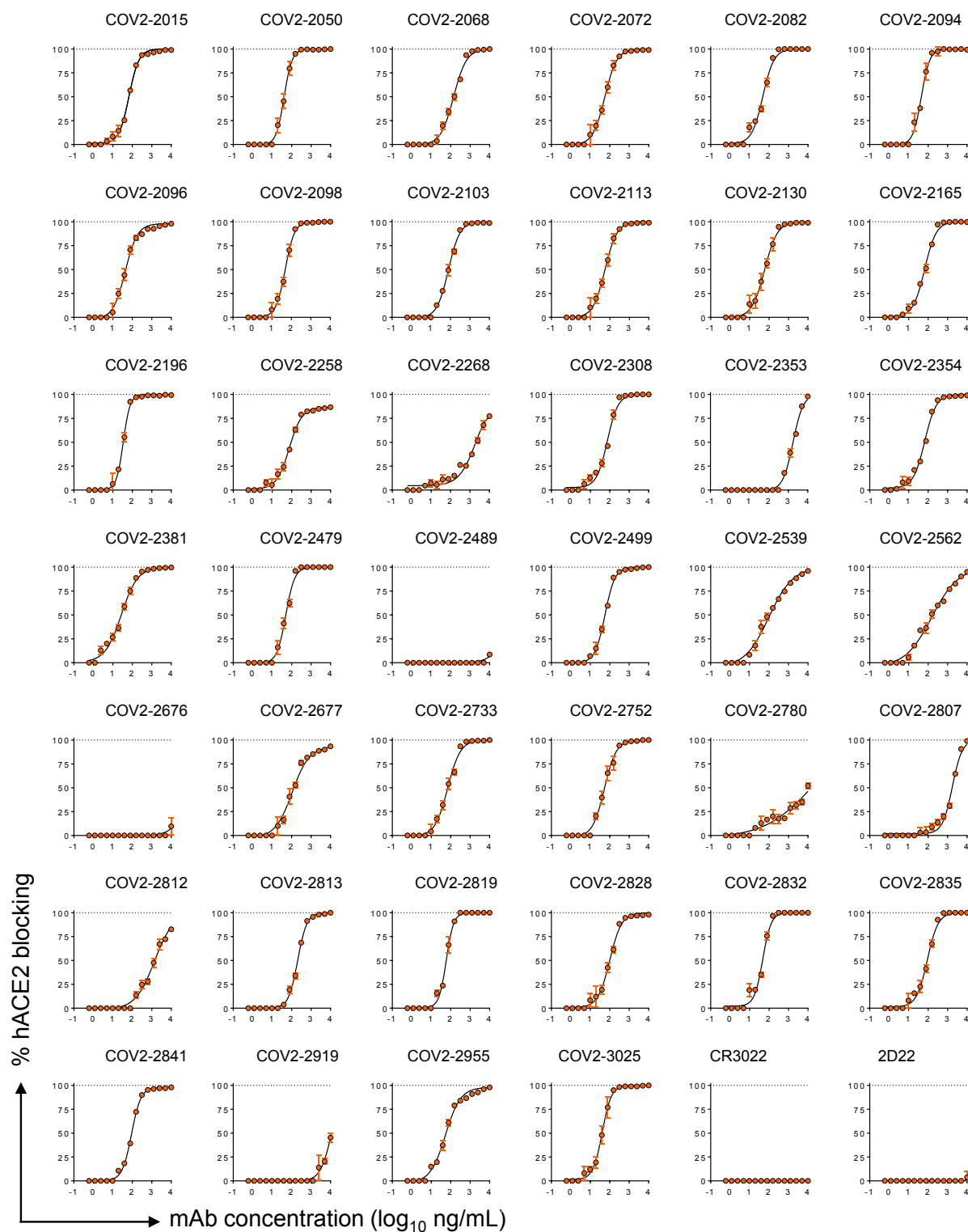# Figure 1

Figure 2

Figure 3

Figure 4

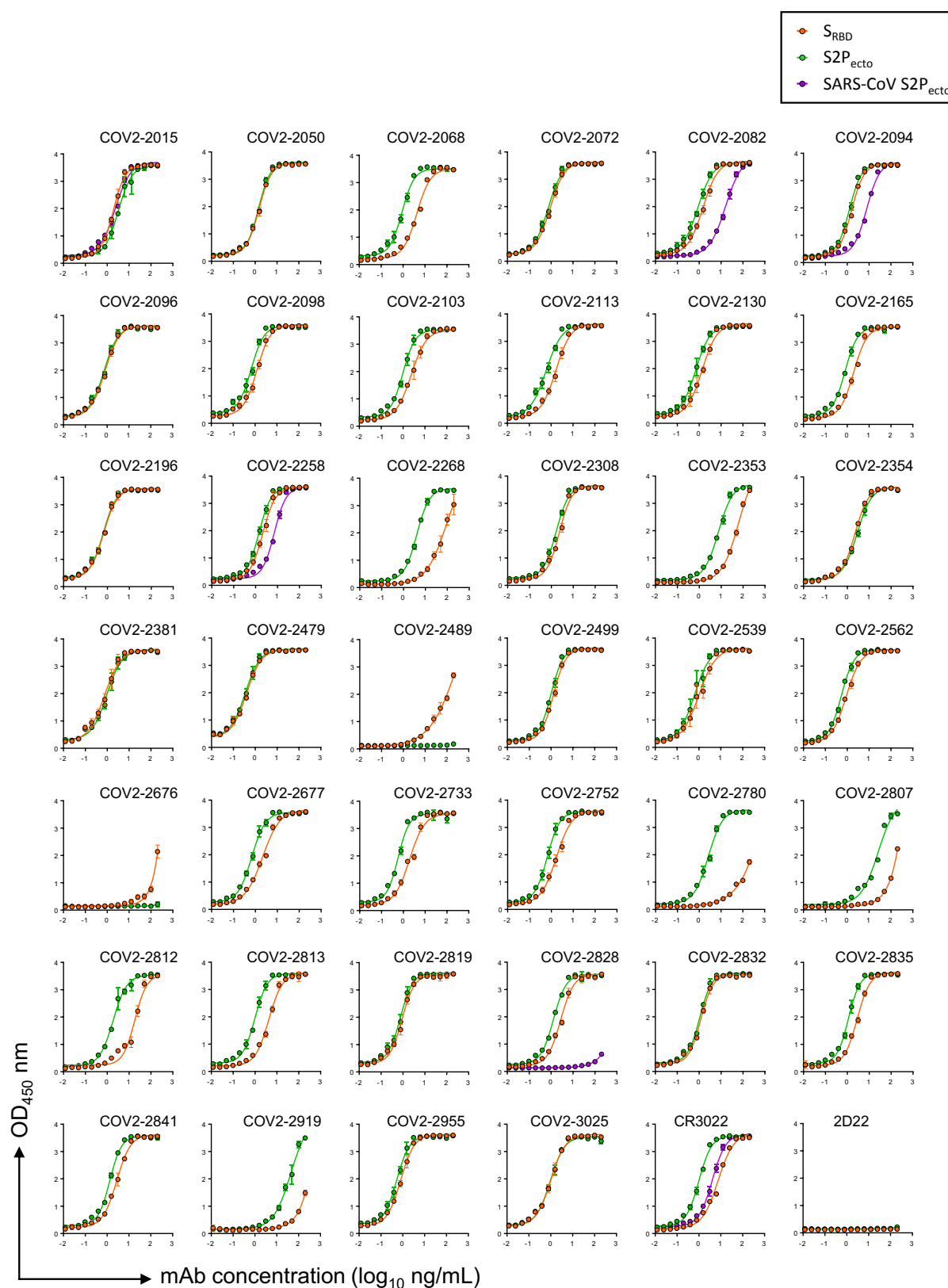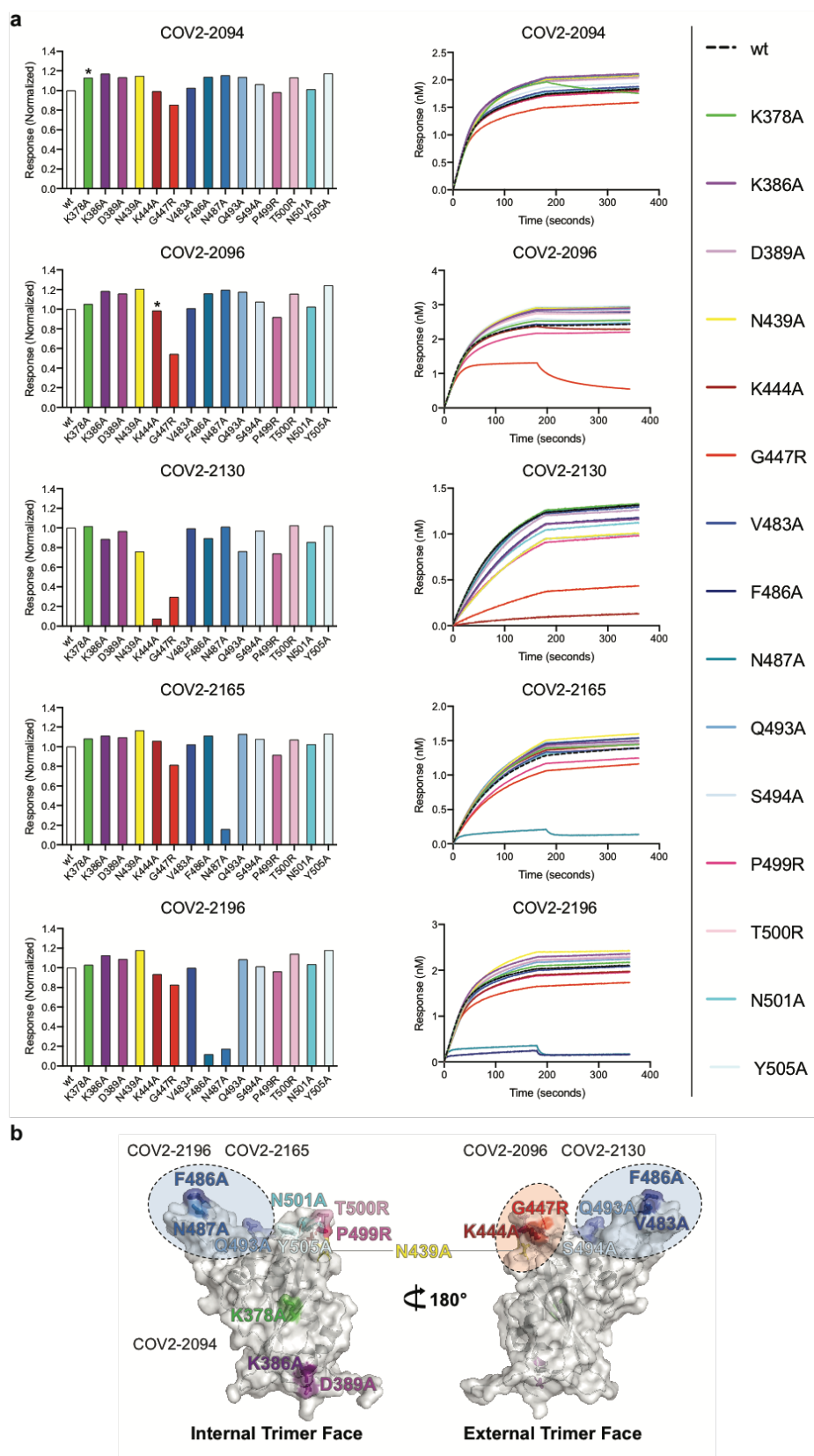**Extended Data Figure 1**

Extended Data Figure 2

Extended Data Figure 3

Extended Data Figure 4

Extended Data Table 1. Neutralization IC$_{50}$, hACE2 blocking IC$_{50}$, and EC$_{50}$ values for binding to S2P$_{ecto}$ or S$_{RBD}$ antigens for mAb panel

MAb	Neutralization IC$_{50}$, ng/mL	hACE2 blocking IC$_{50}$, ng/mL	S2P$_{ecto}$ binding EC$_{50}$, ng/mL	S$_{RBD}$ binding EC$_{50}$, ng/mL	SARS-CoV S2P$_{ecto}$ binding EC$_{50}$, ng/mL
COV2-2015	892	68	2.2	5.1	2.7
COV2-2050	80	63	1.7	1.6	—
COV2-2068	478	166	7.4	1.2	—
COV2-2072	26	29	0.8	1.0	—
COV2-2082	204	43	1.1	0.6	19.9
COV2-2094	154	53	1.8	1.4	11.7
COV2-2096	59	67	1.0	1.0	—
COV2-2098	1,029	48	1.3	0.7	—
COV2-2103	1,969	79	2.9	1.1	—
COV2-2113	1,041	60	1.8	0.6	—
COV2-2130	107	61	1.5	0.7	—
COV2-2165	332	62	1.4	0.6	—
COV2-2196	15	48	1.2	1.1	—
COV2-2258	989	76	2.5	1.6	11.2
COV2-2268	371	2,198	91.2	5.3	
COV2-2308	394	75	2.7	1.9	—
COV2-2353	2,891	1,750	48.0	10.9	—
COV2-2354	1,105	67	2.6	3.5	—
COV2-2381	42	27	0.8	1.0	—
COV2-2489	4,378	—	13.0	—	—
COV2-2479	48	50	0.4	0.3	—
COV2-2499	27	57	1.4	1.1	—
COV2-2539	274	98	1.1	0.7	—
COV2-2562	348	154	1.0	0.6	—
COV2-2676	3,247	—	12.0	—	—
COV2-2677	1,618	107	2.4	0.7	—
COV2-2733	356	71	2.4	0.6	—
COV2-2752	349	53	1.9	0.7	—
COV2-2780	478	10,000	86.0	3.1	—
COV2-2807	907	1,753	13.0	55.1	—
COV2-2812	1,020	1,387	45.4	2.1	—

COV2-2813	555	206	5.3	1.0	—
COV2-2819	114	60	0.9	0.8	—
COV2-2828	100	100	3.2	1.4	338
COV2-2832	70	47	1.3	1.1	—
COV2-2835	190	91	3.4	1.2	—
COV2-2841	1,065	91	3.3	1.5	—
COV2-2919	1,091	1,000	153.0	90.3	—
COV2-2955	127	54	0.8	0.5	—
COV2-3025	37	41	1.1	1.1	—
rCR3022	—	—	10.2	1.1	5.2
r2D22	—	—	—	—	—

— : indicates no detectable binding or neutralization at the highest tested concentration